RSC Advances

ROYAL SOCIETY OF CHEMISTRY

www.rsc.org/advances

Molecular dynamics simulations on dihydroxylammonium 5,5'-bistetrazole-1,1'-diolate/hexanitrohexaazaisowurtzitane cocrystal

Shuling Xiong[a], Shusen Chen[a], Shaohua Jin[a*], and Chunyuan Zhang[a]

Abstract Dihydroxylammonium 5,5′-bistetrazole-1,1′-diolate (TKX-50) is a newly synthesized explosive with high detonation performance, low impact sensitivity and low toxicity. Hexanitrohexaazaisowurtzitane (CL-20), especially Ɛ-CL-20, is currently the highest energy-density explosive. The research on TKX-50/Ɛ-CL-20 cocrystal can improve the defects of single-compound explosives in their application and greatly expand the application range of TKX-50 and CL-20. Seven TKX-50/Ɛ-CL-20 cocrystal models were constructed, and the radial distribution function (RDF), X-ray powder diffraction (XRD) and energy calculation were analyzed based on the equilibrium structures of the cocrysyal models by molecular dynamics (MD) simulations. The results indicate that the diffraction peaks of TKX-50/Ɛ-CL-20 cocrystal quite differ from TKX-50's and Ɛ-CL-20's and new structure forms, hydrogen bond interaction and van der Waals forces exist in the TKX-50/Ɛ-CL-20 cocrystal structure, and the cocrystal model of TKX-50 substituted by Ɛ-CL-20 on its [011] facet is easiest to be formed.

Keywords TKX-50; Ɛ-CL-20; cocrystal; RDF; XRD

1. Introduction

In order to meet the high requirements of modern war and security of new weapons, the research on explosives with high energy storage and low impact sensitivity has become a hot spot.[1-9] Dihydroxylammonium 5,5′-bistetrazole-1,1′-diolate (TKX-50) with excellent comprehensive properties of high energy storage, low impact sensitivity and low toxicity was first synthesized by Fischer in 2012.[10-19] Apart from slightly lower energy-density, its impact sensitivity is much lower than the common explosives and its energy level is higher than the common explosives, which indicates that it possesses promising application prospect in the energetic materials field. Hexanitrohexaazaisowurtzitane (CL-20), especially ε-CL-20, is currently the highest energy-density explosive by far with potential for widespread applications in many weapons, but the high impact sensitivity greatly reduces the security of its application process.[20-21] Thus, the research on modification of TKX-50 and CL-20 single-compound explosives possesses vital significances in the current energetic materials field.

At present, recrystallization, polymer coating and composite methods were usually used to modify the existing single-compound explosives, but these traditional modified methods couldn't change the internal composition and crystal structure of the single-compound explosives themselves, so the modified effects were not ideal. Thus it is an urgent need to develop an effective modified method to meet the development requirements of explosives. Cocrystal is a new modification technology, which combines two or more than two kinds of different types of intermolecular

non-covalent bonds (hydrogen bond, ionic bond, van der Waals force and π-π bond, etc.) into the same lattice, then multicomponent molecular crystal with specific structure and properties forms, it is an equilibrium outcome of thermodynamics, kinetics and molecular recognition, which directly affects the crystal structure.[22-24] Based on the forming principle of cocrystal, if TKX-50/Ɛ-CL-20 cocrystal structure which possesses unique structural features of high energy and low sensitivity forms, it will greatly expand the application range of TKX-50 and CL-20.

TKX-50/Ɛ-CL-20 cocrystal models were constructed based on the designing principle of cocrystal using Material Studio software, and they were optimized by Polymer Consistent Force Field (PCFF) and Smart Minimizer (SM) method. Then we carried out MD simulations on TKX-50/Ɛ-CL-20 cocrystal models to obtain their equilibrium structures. Radial distribution function (RDF), X-ray powder diffraction (XRD) and energy calculation were used to deduce the forming conditions of cocrystal, which provide theoretical basises for the formation of TKX-50/Ɛ-CL-20 cocrystal.

2.   Computational methods

2.1   Crystal morphology prediction of TKX-50

The crystal structure of TKX-50 as shown in Fig. 1 was built based on the single-crystal diffraction data[10] (P_{21}/c space group, Z=2, Monoclinic), then it was optimized by PCFF and SM method. The optimized cell parameters from PCFF are a =5.664Å, b =11.203 Å, c =6.265 Å, and β =99.2°, consistent with the experimental values of a =5.441 Å, b =11.751 Å, c =6.561 Å, and β =95.1° at 300 K[10]. The unit cell

of TKX-50 consists of two bistetrazole anions (formal charge of −2) and four

hydroxylammonium $(NH_3OH)^+$ cations (formal charge of +1) in vacuum.
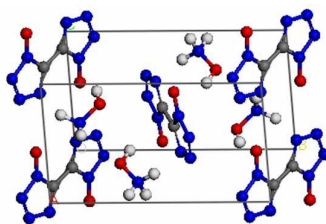
Fig. 1 Crystal structure of TKX-50. The C, H, O, N are represented by gray, white, red, and blue balls,

respectively.

Then we carried out Bravais-Friedel Donnay-Harker (BFDH), Equilibrium

Morphology (EM) and Growth Morphology (GM) methods on the optimized crystal

structure to simulate the crystal morphology of TKX-50 (see Fig. 2). It can be seen

from Fig. 2(a) that TKX-50 possesses five dominant crystal facets and the aspect ratio

is 1.5 using BFDH method and with an aspect ratio of 2.13, TKX-50 presents four

dominant crystal facets by EM method (shown in Fig. 2(b)). Meanwhile, there are six

dominant crystal facets in the crystal morphology of TKX-50 and the aspect ratio of

TKX-50 is 1.97 using GM method (shown in Fig. 2(c)).

The BFDH method is an approximation and does not account for the energetics of

the system, the stronger the bonding effects in the crystal, the less accurate the method

becomes. The EM method is calculated at a temperature of 0 K, it is assumed that the

surface is a perfect termination of the bulk and that no surface relaxation takes place,

thus the calculation of this method is only a theoretical reference value. GM method is

based on the attachment energy method, which attempts to simulate crystal habits as

obtained under non-equilibrium growth conditions. Meanwhile, GM method can

predict the shape of a crystal more accurately than the BFDH method because it takes

the energetics of the system into account. Therefore, we finally chose the simulated

result using GM method as the crystal growth morphology of TKX-50.

(a)   (b)   (c)
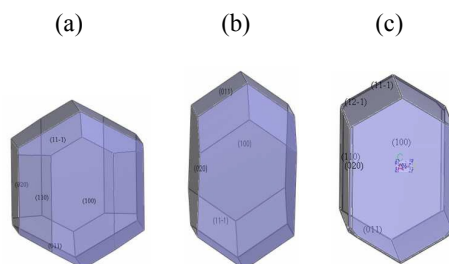
Fig. 2   Crystal growth morphology of TKX-50. Part(a), (b) and (c) were simulated by BFDH, EM and

GM methods, respectivey.

2.2   Constrction of cocrystal models

Hydrogen bonding occupies a vital role in the formation of cocrystal system based on

the forming principle of pharmacy cocrystal.[25-26] TKX-50 contains $(NH_3OH)^+$ cation

and $\mathcal{E}$-CL-20 contains polar nitro group ($-NO_2$), which can form a hydrogen bond of

N-O...H type. The molecular structures of TKX-50 and $\mathcal{E}$-CL-20 and the formative

hydrogen bond are shown in Fig. 3. Then we constructed the ($2\times2\times1$) supercell

structure of TKX-50 and supramolecular structure of TKX-50/$\mathcal{E}$-CL-20 cocrystal with

molar ratio of 2:1. Cocrystal models of TKX-50 substituted by $\mathcal{E}$-CL-20 were divided

into random substitution and six different growth crystal facets substitution, a total of

seven kinds of cocrystal models were finally constructed.

$\mathcal{E}$-CL-20
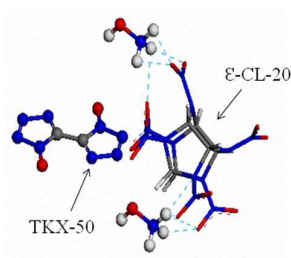
TKX-50

Fig. 3 Molecular structures of TKX-50 and Ɛ-CL-20. TKX-50 and Ɛ-CL-20 are represented by ball

model and stick model, respectively. Dotted lines represent hydrogen bond.

2.3 MD simulations of cocrystal models

These cocrystal models were optimized by SM method to eliminate the unreasonable

energy and conformation in the supercells. Then we carried out MD simulations on

these seven kinds of cocrystal models to obtain their equilibrium structures. The MD

time step was 1 fs and the temperature control method was set following Velocity

Scale. Electrostatic and van der Waals interactions were calculated by Ewald's and

Atom-based methods, respectively. An MD simulation with a total simulation time of

100ps was used for equilibrating the simulated system. When the simulated system

has reached its equilibration stage, that is, the fluctuation of the temperature and

energy around their averages was below 5%, we carried out another MD simulation

with a period of 100ps. A total of 2,000 frames were finally collected at an interval of

50 fs. One of the final equilibrium structures of TKX-50/Ɛ-CL-20 cocrystal models is

shown in Fig. 4.
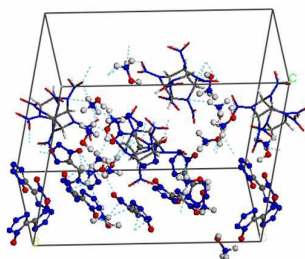
Fig. 4 Equilibrium structure of TKX-50/ Ɛ-CL-20 cocrystal model.

2.4 XRD simulation

To deduce the formation of cocrystal structure, we carried out XRD simulation on the

equilibrium configurations of TKX-50/Ɛ-CL-20 cocrystal models using reflex module.

Cu target was selected, scanning range was $5^0 \sim 45^0$ and the step size was 0.02fs.

2.5 RDF simulation

RDF usually refers to the distribution probability of the other particles in the space when the coordinates of a particle are given. Therefore, RDF can be used to study the material order and describe the electron correlation. In order to further clarify the TKX-50/Ɛ-CL-20 cocrystal structure and the nature of intermolecular force, we carried out RDF simulations on the TKX-50/Ɛ-CL-20 cocrystal structures which were calculated by MD simulations using forcite module.

3. Results and discussion

3.1 Analysis of dominant crystal facets of TKX-50

According to the crystal morphology of TKX-50 simulated by GM method, the main growth facets of TKX-50 are shown in Table 1. TKX-50 possesses six dominant crystal facets: [100], [011], [020], [110], [11-1] and [12-1] facets, the [011] facet which occupies the largest area percentage exhibits the most morphological importance. [100], [011] and [020] facets with larger interplanar spacing (d_{hkl}) are the slow-growing facets and other facets which possess smaller d_{hkl} are the fast-growing facets. With no hydrogen bonding interaction, the attachment energy, E_{att}, mainly composes of electrostatic interaction and van der Waals forces.

Tabel 1   Dominant crystal facets of TKX-50

Facet	Multiplicity	d_{hkl}/Å	E_{att}(total) (kJ·mol^{-1})	E_{att}(vdW) (kJ·mol^{-1})	E_{att}(Electrostatic) (kJ·mol^{-1})	E_{att}(H-bond) (kJ·mol^{-1})	Total facet percentage(%)
[100]	2	5.581	-45.167	-21.266	-23.901	0	33.164

[020]	2	5.595	-41.988	-24.541	-17.446	0	28.616
[011]	4	5.293	-53.993	-15.046	-38.947	0	35.551
[110]	4	4.994	-58.049	-26.378	-31.671	0	1.750
[11-1]	4	4.186	-75.482	-23.001	-52.481	0	0.620
[12-1]	4	3.513	-74.340	-26.791	-47.550	0	0.300

3.2 Energy calculation of cocrystal system

As the E_{att} calculation results shown in Table 2, the E_{att} results of cocrystal models of TKX-50 substituted by ϵ-CL-20 on its slow-growing facets are lower, which shows that these formative cocrystal structures are more stable. What's more, with the lowest E_{att} result, [011] facet/ϵ-CL-20 cocrystal structure is easiest to be formed.

Tabel 2 E_{att} of cocrystal models

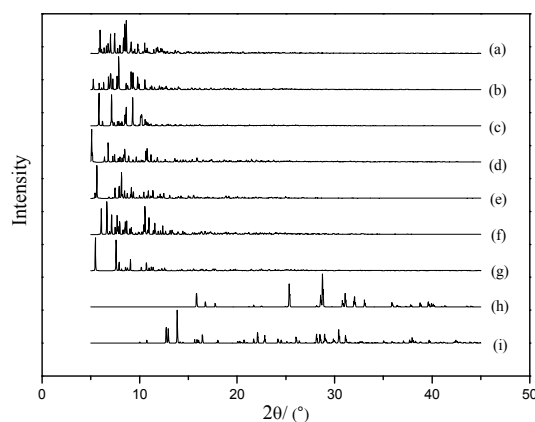| Cocrystal models	[011][a]	[100][b]	[020][c]	[110][d]	[12-1][e]	[11-1][f]
E_{att} (kcal·mol^{-1})	-810.79	-774.30	-750.21	-547.75	-463.36	-426.88

[a][011] facet/ϵ-CL-20 cocrystal, [b][100] facet/ϵ-CL-20 cocrystal, [c][020] facet/ϵ-CL-20 cocrystal, [d][110] facet/ϵ-CL-20 cocrystal, [e][12-1] facet/ ϵ-CL-20 cocrystal, [f][11-1] facet/ ϵ-CL-20 cocrystal.

3.3 XRD analysis

XRD spectra of TKX-50/ϵ-CL-20 cocrystal models are shown in Fig. 5. It can be seen in the XRD diffraction peaks that characteristic peaks of TKX-50's and ϵ-CL-20's nearly disappeared and new diffraction peaks appeared between 5^0 and 10^0 in the cocrystal models. What's more, the emergence of new diffraction peaks and the disappearance of characteristic peaks were not the simple superposition of diffraction peaks from TKX-50's and ϵ-CL-20's. The position and intensity of XRD peaks are related to object phase, size of crystal and the arrangement of crystal in structural motif. Any kind of object phase possesses specific interplanar crystal spacing and

characteristic value of diffraction intensity. For structures of different object phases, the diffraction intensity and diffraction position of the diffraction peaks are also different. Therefore, TKX-50/ℰ-CL-20 cocrystal system was proved to be a new crystal structure which possesses new lattice parameters based on the disappearance of characteristic peaks or the decrease of the peak intensity and the appearance of new diffraction peaks. This is the crystal structures of TKX-50's and ℰ-CL-20's were destroyed by hydrogen bonding interaction and van der Waals forces in the process of their cocrystal formation, thus, a new structure formed.


Fig. 5   XRD spectra of (a) [12-1] facet/ℰ-CL-20, (b) [11-1] facet/ℰ-CL-20, (c) [110] facet/ℰ-CL-20, (d) [100] facet/ℰ-CL-20, (e) [020] facet/ℰ-CL-20, (f) [011] facet/ℰ-CL-20, (g) TKX-50/ℰ-CL-20, (h) TKX-50 and (i) ℰ-CL-20.

3.4   RDF analysis

RDF is usually represented by g (r, r'), for the relatively small |r-r'|, g(r, r') mainly characters the accumulation state of atoms and the distance between each bond. For the nature of long range, the probabilities of finding atoms are basically the same for a given distance, so g (r, r') flattens out with the increase of |r-r'| and finally tends to a

constant value. Usually, the intermolecular forces include hydrogen bond interaction and van der Waals forces, the length ranges of hydrogen bond, strong van der Waals forces and weak van der Waals forces are 0.110nm~0.310nm, 0.310nm~0.503nm and greater than 0.503nm, respectively.

As the RDF spectra shown in Fig. 6, there is a peak near r=0.22nm in each spectrum, indicating that the hydrogen bonds are formed by the hydrogen atoms of TKX-50 and the oxygen atoms of Ɛ-CL-20. By comparison, the lower E_{att} the facet possesses, the stronger the intensity of peak value of its cocrystal model exhibits, so the strongest hydrogen bond forms in the [011] facet/Ɛ-CL-20 cocrystal model. Meanwhile, there is also a peak near r=0.32nm in each spectrum, which shows that the strong van der Waals forces also exist in each cocrystal model. Hydrogen bonding and van der Waals forces which destroy the crystal structures of TKX-50 and Ɛ-CL-20 are the necessary conditions for the formation of cocrystal.

(a)

(b)

(c)

(d)

(e)   (f)
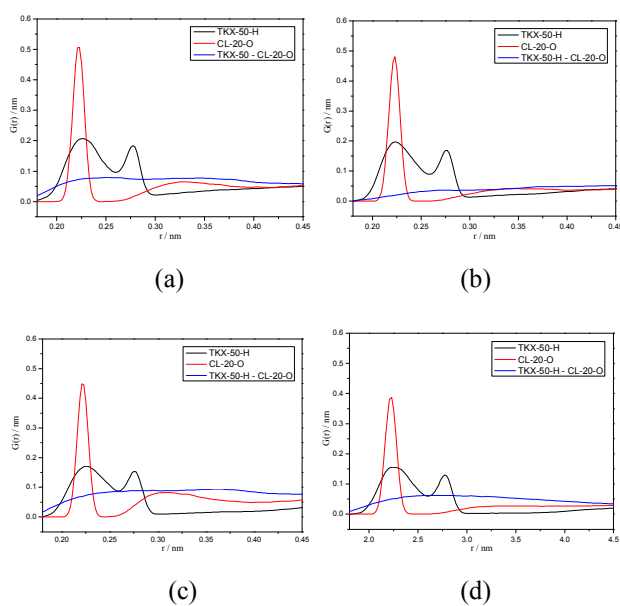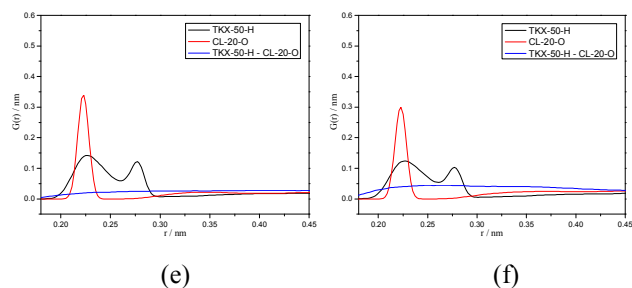
Fig. 6   RDF spectra of (a) [011] facet/Ɛ-CL-20, (b) [100] facet/Ɛ-CL-20, (c) [020] facet/Ɛ-CL-20, (d)

[110] facet/Ɛ-CL-20, (e) [11-1] facet/Ɛ-CL-20 and (f) [12-1] facet/Ɛ-CL-20.

4.   Conclusions

The XRD diffraction peaks of TKX-50/Ɛ-CL-20 cocrystal quite differ from TKX-50's

and Ɛ-CL-20's and new peaks appear in the cocrystal model, indicating that the crystal

cell parameters of cocrystal structure have changed and TKX-50/Ɛ-CL-20 cocrystal

structure with more excellent comprehensive properties has been proved to form

which possesses the advantages of both TKX-50 and CL-20 and improves the defects

of them at the same time, this new crystal will solve the limitation problems of

TKX-50 and CL-20 in their application process caused by their defects, so TKX-50

and CL-20 can be early applied to the energetic materials field by this method.

   Hydrogen bonding and van der Waals forces were proved to exist in the

TKX-50/Ɛ-CL-20 cocrystal structure by RDF spectra, which are the necessary

conditions for the formation of cocrystal. The E_{att} results of cocrystal models of

TKX-50 substituted by Ɛ-CL-20 on its slow-growing facets are lower, which shows

that the cocrystal structures of these facets are more stable. The E_{att} of [011]

facet/Ɛ-CL-20 cocrystal is the lowest, indicating that the cocrystal model of TKX-50

substituted by Ɛ-CL-20 on its [011] facet is easiest to be formed. The design, forming

conditions and action mechanism of TKX-50/ε-CL-20 cocrystal not only provide theoretical basises for the formation of cocrystal, but also possess important significance in the improvement of modified technique of single-compound explosive crystal.

Notes and references

1 T. M. Klapötke, A. Preimesser and J. Stiertorfer, *Zeitschrift für Anorganische und Allgemeine Chemie,* 2012, **638**, 1278−1286.

2 R. Duddu, P. R. Dave, R. Damavarapu, N. Gabler and D. Parrish, *Tetrahedron Letters*, 2010, **51**, 399−401.

3 R. Wang, H. Xu, Y. Guo, R. Sa and J. M. Shreeve, *Journal of the American Chemical Society*, 2010, **132**, 11904–11905.

4 A. K. Sikder and N. Sikder, *J. Hazard. Mater,* 2004, **112**, 1−15.

5 M. B. Talawar, R. Sivabalan, M. Anniyappan, G. M. Gore, S. N. Asthana and B. R. Gandhe, *Comb., Explos.*, *and Shock Waves*, 2007, **43**, 62−72.

6 M. B. Talawar, R. Sivabalan, T. Mukundan, H. Muthurajan, A. K. Sikder, B. R. Gandhe and A. S. Rao, *J. Hazard. Mater*, 2009, **161**, 589−607.

7 O. Bolton and A. J. Matzger, *Angew. Chem., Int. Ed*, 2011, **50**, 8960−8963.

8 A. A. Dippold and T. A. Klapötke, *J. Am. Chem. Soc*, 2013, **135**, 9931−9938.

9 Q. An, H. Xiao, W. A. Goddard and X. Y. Meng, *J. Phys. Chem. Lett*, 2014, **5**,

485−489.

10 N. Fischer, D. Fischer, T. M. Klapötke, D. G. Piercey and J. Stierstorfer, *Journal of Material Chemistry*, 2012, **22**, 20418–20422.

11 N. Fischer, T. M. Klapötke, M. Reymann and J. Stierstorfer, *European Journal of Inorganic Chemistry*, 2013, **12**, 2167–2180.

12 N. Fischer, T. M. Klapötke, M. A. Matecic, J. Stierstorfer and M. Sucesca, *New Trends in Research of Energetic Materials*, 2013, **16**, 574–585.

13 V. K. Golubev and T. M. Klapötke, *New Trends Res. Energ. Mater., Proc.Semin., 17th*, 2014, **1**, 220−227.

14 V. K. Golubev and T. M. Klapoetke, *New Trends Res. Energ. Mater., Proc. Semin., 17th*, 2014, **2**, 672−676.

15 Q. An, W. G. Liu, W. A. Goddard, T. Cheng, S. V. Zybin and H. Xiao, *J. Phys. Chem. C*, 2014, **118**, 27175−27181.

16 Q. An, T. Cheng, W. A. Goddard and S. V. Zybin, *J. Phys.Chem.C*, 2015, **119**, 2196−2207.

17 B. Yuan, Z. J. Yu and E. R. Bernstein, *J. Phys. Chem. A*, 2015, **119**, 2965−2981.

18 Z. A. Dreger, Y. C. Tao, B. B. Averkiev, Y. M. Gupta and T. M. Klapötke, *J. Phys. Chem. B*, 2015, **119**, 6836−6847.

19 H. F. Hang, Y. M. Shi, J. Yang and B. P. Li, *Journal of Energetic Materials*, 2015, **33**, 66–72.

20 Y. Kholod, S. Okovytyy, G. Kuramshina, M. Qasim, L. Gorb and J. Leszczynski, *J. Mol. Struct*, 2007, **843**, 14– 25.

21 X. J. Xu, W. H. Zhu and H. M. Xiao, *J. Phys. Chem. B*, 2007, **111**, 2090– 2097.

22 J. M. Thomas, *Cryst Eng Comm*, 2011, **13**, 4304-4306.

23 H. N. Rodriguez, S. J. Nehm, K. F. Seefeldt, T. Y. Pagan and C. J. Falkiewicz, *Mol Pharm*, 2006, **3**, 362-367.

24 A.V. Trask, W. D. S Motherwell and W. Jones, *Cryst Growth Des*, 2006, **5**, 1013-1021.

25 S. L. Morisstte, O. Almarsson, M. L. Peterson, J. F. Remenar, M. L. Read, A. V. Lemmo, S. Ellis, M. J. Cima and C. R. Gardner, *Advanced Drug Delivery Review*, 2004, **3**, 275-300.

26 A. Jayasankar, A. Somwangthana, Z. J. Shao and N. Rodriguez-Hornedo, *Pharm Res*, 2006, **23**, 2381-2392.